

Separation Force Analysis based on Cohesive Delamination Model for Bottom-up Stereolithography Using Finite Element Analysis

Farzad Liravi

Department of Industrial and Systems Engineering
University at Buffalo, The State University of New York, Buffalo, NY 14260

Sonjoy Das

Department of Mechanical and Aerospace Engineering
University at Buffalo, The State University of New York, Buffalo, NY 14260

Chi Zhou*

Department of Industrial and Systems Engineering
University at Buffalo, The State University of New York, Buffalo, NY 14260

*Corresponding author: chizhou@buffalo.edu, (716) 645-4706

ABSTRACT

Bottom-up (constrain-surface) Additive Manufacturing (AM) systems have been widely used in industry. Compared to traditional open-surface AM technology, properties like better vertical resolution, higher material filling rate, less production time, and less material waste make bottom-up AM technology a suitable candidate for fabrication of complex three dimensional materials with high accuracy. However during the pulling up stage, the substantial force generated between the formed part and the material container has high risk of breaking the part and therefore reduces the process reliability. In this paper, an optimization-based method is developed to model bottom-up AM process using finite element analysis (FEA). The FEA model is developed using ABAQUS to model the behavior of the cohesive delamination at the interface of the formed part and a hyper-elastic intermediate which has been used to reduce the pulling up force. An optimization model is also established to evaluate the cohesive stiffness parameters that cannot be calculated directly from closed formulas or mechanical tests. The results of this work will be used to develop an adaptive closed-loop mechanics-based system to control the pulling up process and achieve a reliable technology.

1. INTRODUCTION

Additive Manufacturing (AM) is a new manufacturing technology that fabricates complex three dimensional objects by adding materials layer upon layer. In a recent special report of the Economist magazine, AM was hailed as the third industrial revolution [1]. However, despite all the significant advancements of AM technology [2], especially in the last decade, some technical challenges, e.g. poor surface quality, high machine cost, low reliability and reproducibility, and limited compatible materials still need to be addressed. As a result, Additive Manufacturing processes need to be modified for faster and cheaper fabrication of solid free form (SFF) objects. Novel solutions for improving the AM processes have been proposed by researchers. Investigating different materials and parameters, combining different processes, and applying various post-processing techniques are amongst these solutions. However, most of them are still in the trial and error level and the main reason is the lack of research on the physical modeling and related optimization methods. As a result, there is an urgent need to address these challenges in order to promote AM wide adoption and achieve the full industrial revolution.

Among different AM technologies, the focus of this paper is on bottom-up image-projection-based Stereolithography (SLA). SLA is a photopolymerization-based AM process and also the first commercialized AM technology. Compared to other additive manufacturing techniques, solid parts fabricated using SLA have the highest accuracy and the best surface quality. As one of the most important factors in this technique, material filling mechanism directly affects the throughput and reliability of the process. Two most widely used material filling mechanisms are top-down (free-surface) and bottom-up (constrain-surface). Bottom-up process can achieve better vertical resolution and higher material filling rate and is more widely used in practice.

The differences between these two mechanisms are in the build orientation and the method of polymer curing. Fig. 1(a) shows a top-down projection-based Stereolithography system. In top-down Stereolithography, a pattern is fabricated on the surface of the resin using a computer controlled laser beam or a digital light projector. The resin exposed to light is solidified to a defined pattern and will be adhered to the platform. After the first layer is cured, the platform is moved down and the surface is recoated with liquid resin. This process is repeated until the fabrication of solid object is completed. However, in the bottom-up process, the light source

is under the resin vat. As a result, light is projected on a transparent plate which is the bottom of the resin vat from the underneath. The platform is dipped into the resin from the above and the first layer will be cured in the gap between the platform and the vat bottom and adhered to the platform. After each layer is fabricated, the platform first moves up for the amount of h and then dips down for $h - \text{layer thickness}$. The resin will flow into the gap again and the next layer will be built. Fig. 1(b) shows a typical bottom-up projection-based Stereolithography system. Newly developed SLA systems use Digital Micro-mirror Device (DMD, *Texas Instruments*, Dallas, TX) as the light source. A DMD can be considered as a semiconductor light switch. It is composed of thousands of tiny, squared, $16 \times 16 \mu\text{m}$ micro mirrors. Each mirror is able to switch on or off a light pixel which are corresponding to pure white and black pixels. Since the mirror can switch on and off more than 1000 times per second, this rapid speed allows digital gray scale and colorful pixels generated. DMD acts as a dynamic mask generator, as the micro-mirrors are tilted to the on or off positions to produce 2D images which are the results of sliced 3D geometry. For each layer, the illuminated area is solidified simultaneously under one irradiation once exposed to UV or visible light, while the dark region remains liquid.

The bottom-up approach has several advantages over the top-down process and is being used increasingly:

- There is no need to recoat the surface with resin as the recoating happens automatically as the platform moves down. However, the moving down process should be controlled itself so that the resin flow into the gap is completed. An incomplete resin flow affects the surface quality and mechanical properties of the final part.
- The required amount of photopolymer resin is much less than the top-down approach. This results in the less waste of the expensive photopolymer. Zhou et al. have taken advantage of this property to design a multi-material photopolymerization-based AM system [3].
- The cured surface is always smooth as it is compressed between the building platform and the bottom of the resin tank during moving up and dipping down movements.
- The layer is fabricated in the resin, so it is not exposed to oxygen and the oxygen inhibition is eliminated. Hence the liquid photopolymer can be cured faster by eliminating the oxygen inhibition effect [4].
- The container depth is independent of the part height. Thus a shallow vat can be used to reduce the required volume of liquid photopolymer.
- Much smaller layer thickness can be achieved since the gap size is only determined by the Z stage resolution regardless of the fluid properties of the liquid resin. Therefore, much higher vertical resolution and better surface quality can be accomplished.

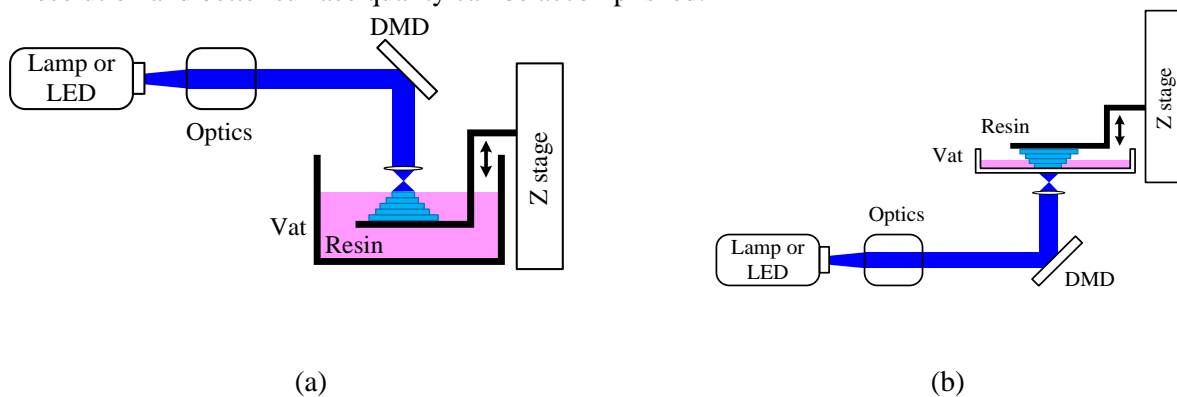


Figure 1. Comparison of (a) top-down projection-based Stereolithography; (b) bottom-up projection-based Stereolithography.

Despite all the advantages, solids built by bottom-up SLA systems are subject to larger mechanical forces, as they have to be separated from the bottom of the resin tank after each layer is cured. The large amounts of pulling-up force can cause damage to the curing part and may break it (Fig. 2). To mitigate this problem, substantially slow motion and long waiting time are set to improve the reliability. However, the result is a very slow and inefficient process. In order to fundamentally solve this problem, an adaptive mechanics-based process must be investigated and developed to achieve the best reliability and through-put.

The objective of this research work is to systematically study the fundamental principles and mechanism of the separation and accordingly present a predictive methodology and in-situ feedback control system to substantially improve the through-put and reliability of the bottom-up projection-based additive manufacturing process. In this paper, the cohesive interface between the built parts (e.g. solidified photopolymer) and the media (e.g. Silicone film) is modeled by having recourse to mechanical-based interface concept, Cohesive Zone Model (CZM) to accurately account for the effects of the separation mechanism. In addition, finite element methods will be used to investigate the relation between motion profile and the crack initialization and propagation during the separation process.



Figure 2. The failure in production of a hearing aid via bottom-up Stereolithography due to excessive pulling-up force.

An optimization-based method is also presented for evaluation of the mechanical parameters associated with the cohesive behavior. These parameters known as cohesive stiffness parameters cannot be calculated directly from closed formulas or mechanical tests. The outcome of the proposed research can also advance the knowledge and understanding of the material filling mechanism since it will be rigorously founded on the concepts of the solid mechanics and fracture mechanics.

The separation between the cured part and the base media during the pulling-up process is dynamically shown in Fig. 3 (a~d). The cured layer is sandwiched between the previously built layer and the top surface of the media as shown in Fig. 3(a). As the part moves up with the platform, the media begins to deform and separation (crack) begins to initiate at the boundary area of the interface as shown in Fig. 3(b). In Fig. 3(c), the separation propagates into interior area while the platform continues moving up. The separation is completed after the platform moves enough distance, as shown in Fig. 3(d).

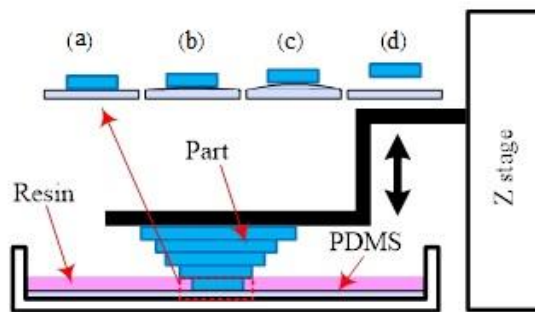


Figure 3. The separation process in bottom-up SLA; (a) layer is cured and sandwiched between the previous layers and the vat bottom; (b) crack is initiated at the interface of layer and vat bottom; (c) crack is propagated as the platform moves up; (d) the complete delamination happens.

During the pulling-up stage, the cured layer might not levitate together with the above layers and stay on the bottom of the resin tank. As a result, the part will break and should be fabricated from the beginning. One approach to conquer the attachment force is to increase the exposure to significantly over-cure the current layer such that its bonding force with previous layer can be increased. However, at the same time, the bonding force with the vat surface is also increased. Furthermore, over-curing can lead to poor surface quality and inaccurate dimensions. Another approach to address this problem is to apply a certain type of coating to the resin vat so that the attachment force of a cured layer will be reduced. Suitable coatings including Teflon and Silicone films can help the separation of the part from the vat [3, 5]. *Denken* and *EnvisionTec* have used a coated Teflon glass as a media. *Denken Co.* has developed DLP system which works based on bottom-up Stereolithography. DLP system uses two solutions to break the vacuum between the curing layer and vat bottom. First, using a coated Teflon glass as the resin tank and second, scanning the surface of the layer in a large scanning pitch that will have partial cured resin between scanning lines. The partially cured resins will

produce elastic and shear strength properties that ease breaking the vacuum at the interface of the cured layer and the resin vat. The Teflon also makes the separation easier. However, using both these solutions, still the required pulling force is very big and may damage the cured part [6]. Another bottom-up system was developed by *Autostrade* [7]. The performance of this system called EDARTS is similar to DLP. However, instead of Teflon, a layer of silicone film has been used as an intermediate between the part and the resin vat. The silicone-film is a hyper-elastic material that provides both suitable mechanical properties, e.g. shear strength, and the separation ability. In addition to suitable properties, using silicone film eliminates the need for large scanning pitch, as a result, we have used a type of silicone film called Polydimethylsiloxane (PDMS, Sylgard 184, Dow Corning Co.) in this research work.

Huang and Jiang investigated the attachment force of the coating of an elastic silicone film and developed a direct mask curing system that uses silicone film to separate the curing part easily as the platform moves up [5]. They proposed the degree of cure and the area of cure as influential factors on pulling force. The reason is that after the solidification of a layer, the gap between the silicone film and the cured part becomes vacuum state, so a pulling force occurs when the platform is moving up. They have also designed a measurement system to analyze the pulling force. They utilized a load cell which is connected to both the platform and elevator of z-axis. A computer collects the real voltage as the platform moves up and an experiment was conducted by them to find the relationship of real pulling force and the voltage value.

EnvisionTec developed another approach in its *Perfactory Systems* to reduce the large attachment force. They incorporated additional mechanisms to add tilting motions in the part separation, i.e. one side of the platform can be moved up slowly before the other side during the separation. As a result, the part can be peeled off from the vat surface instead of being pulled up and the detaching force will be significantly reduced. However, this method can only work for the cases where the parts are located close to the tilting side. The proposed method may fail if the parts are large or they are located close to the pivot axis. The additional tilting motion will also increase the fabrication time. The result of their work shows that using other approaches for detaching the part from the resin vat rather than the direct pulling up in normal direction may decrease the amount of detachment forces. A two-channel system [3] and a two-way linear motion system [8] have been proposed based on this fact and have significantly reduced the separation force between the cured later and the resin vat.

The two-channel system introduced by Zhou et al. [3] was utilized by an open-source personal 3D printer (B9 Creator). They first came up with a new measure system to investigate the pulling-up force. In their measurement system, two flexible sensors (Tekscan, South Boston, MA) with a range of 0-25 lbs are sandwiched between the fixture and vat. Since the vat is free at the bottom and the side, and only fixed at the top, the pulling force by the part will be transferred to the sensors when the platform levels up. The two sensors are connected to a microcontroller, which can sample and record the sensor readout in over 50 Hz. They ignored the first 25 layers and began to record the separation force after that. They designed experiments to investigate the effects of three important factors on the separation force: (1) exposure time; (2) image area; (3) image shape. The result of their work shows that the image shape has some effects on the peak force but not as significant as the exposure time and the projection area. Their work also showed that even using coated PDMS film on the vat, the separation force is still considerably large (~100 oz or 27.8 N for an image area of 625 mm² with 1 second exposure). It also authenticates the necessity of designing a more solid on-line monitoring system. Having an efficient measurement system, Zhou et al. introduced the two-channel design and used PDMS silicone film as an intermediate. They introduced a photolithography-based micro-fluid technique for continuously fabricating polymeric particles. The developed technique is based on the oxygen-aided inhibition near the PDMS surfaces to form chain-terminating peroxide radicals. As a result, a very thin oxygen inhibition layer will be formed that can prevent cured layer attach to the PDMS film. The oxygen-aided inhibition around the PDMS surface leaves a non-polymerized lubricating layer. Hence, the cured layer can easily slide on the PDMS surface. Based on this property, they apply a transparent PDMS film on half of the bottom surface of a transparent glass vat dividing it into two channels: with and without PDMS coating. A mask image will be only exposed on the channel with PDMS. After a layer is cured, the vat will be translated in x-axis such that the part will be moved to the channel without PDMS and the vacuum will be broken. Hence, if the PDMS film is thick enough (> 0.5 mm), the part can be easily separated from the vat. After moving up the part by a certain distance d , the vat is moved back such that the part is on top of the channel with PDMS. Finally the platform will move down by a distance of $d - \text{layer thickness}$. They repeated the calculation of the pulling-up force using the same measurement system with a small modification so it can measure the shearing force. The results show that the peak separation forces are relatively small (around 2-4 oz or ~ 0.83 N) which are only 4-5% of the related ones observed in the conventional one-channel system. However, Two-channel system and systems

similar to it reduce the amount of pulling force, they require two extra motions in x-direction which will dramatically slow down the building speed. In addition half of the resin vat remains unused resulting in material and space waste.

To remove the extra motion for tilting and sliding, the direct pulling approach is used by *EnvisionTec* in its *Ultra²* and *Micro Printer Systems*. The common strategy used to conquer the large separation force is to move the platform up very slowly and allow the separation to be successfully initiated and then propagated. However, this strategy cannot be reliably applied to more intricate parts with multi-scale features. Furthermore, the slow moving speed reduces the building speed. Attributed to high accuracy and fast speed, bottom-up projection-based additive manufacturing process is widely used in mass customization applications e.g. medical (*Siemens Inc.*) and dental area (*Invisalign Inc.*). However, the drawbacks and challenges associated with this process hinder the further development of this technology. As a result, there is an urgent need to attack these challenges in order to more efficiently and effectively promote its wide adoption to various industries.

2. MODELING COHESIVE DELAMINATION

Different methods have been used for the simulation of delamination using Finite Element Analysis. Virtual Crack Closure Technique (VCCT) and Cohesive Zone Model (CZM) are the most popular methods used for this purpose.

In VCCT, the assumption is that the energy release during delamination is equal to the work required to close the crack back to its original position [9]. This technique has been provided in ABAQUS packages and can be used in ABAQUS/Standard to analyze brittle interfacial crack propagation due to delamination or debonding. It is a post-processing and remeshing technique that provides progressive crack growth between bonded surfaces based on the fracture toughness of the bond and the strain energy release rate at the crack tip. However, VCCT is a powerful technique for modeling delamination and computing strain energy release rate (SERR), but it has some disadvantages that make it hard to use in our case. It is useful for sharp cracks and linear elastic materials, but in reality neither sharp crack nor linear elastic materials exist. This model also requires calculation of fracture parameters, e.g. stress intensity factors or SERR which require nodal variable and topological information from the nodes ahead and behind the crack front. These calculations can be really tedious for the cases in which the crack propagation is involved [10].

Cohesive Zone Model (CZM) properties, however, make it a suitable candidate for our purpose. CZM has been extensively used for simulation of delamination [11-19]. The assumption in this methodology is that a cohesive damage zone develops near the crack top. This delamination modeling method links the microstructural failure mechanism to the continuum fields governing bulk deformations. Thus, it is characterized by the properties of bulk materials, the crack initiation, and the crack evolution function [10]. Cohesive damage zone model relates cohesive surface traction to displacement or separation at the interface where a crack may occur which is called traction-separation model. CZM can be modeled in ABAQUS in two ways: (1) cohesive elements method; (2) surface-based cohesive behavior. The surface-based cohesive behavior is primarily intended for situations where the thickness is negligibly small. In our case, the thickness of the cohesive layer is zero, therefore the surface-based cohesive model can be used to best characterize the bonding property of the intermediate material. Both of these methods follow traction-separation model. Figure 4 shows a bilinear traction-separation model. This model assumes initially a linear elastic behavior and after that the delamination progresses by initiation and evolution of damage. The elastic-constitutive matrix relating normal and shear stresses to the normal and shear separations across the interface is shown in Eq. 1.

$$t = \begin{Bmatrix} t_n \\ t_s \\ t_t \end{Bmatrix} = \begin{bmatrix} K_{nn} & K_{ns} & K_{nt} \\ K_{ns} & K_{ss} & K_{st} \\ K_{nt} & K_{st} & K_{tt} \end{bmatrix} \begin{Bmatrix} \delta_n \\ \delta_s \\ \delta_t \end{Bmatrix} = K\delta \quad (1)$$

Where K is the stiffness parameters matrix and t is the nominal traction stress vector which consists of three components (two components in two dimensional problems): t_n , t_s , t_t , which represent the normal and two shear tractions, respectively. The corresponding separations are denoted by δ_n , δ_s , and δ_t . In our case, the only values that matter are the ones in the normal direction, because our object is only moving in the normal direction. Thus, our model can be considered a pure mode I delamination.

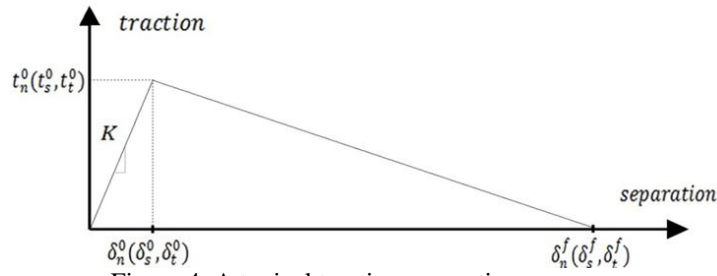


Figure 4. A typical traction-separation response

Damage initiation is related to the interfacial strength, i.e. the maximum traction on the traction-separation model. Once the amount of traction reaches the critical point, crack starts to grow. Many laws, however, have been proposed to govern constitutive equations for crack or delamination growth, e.g. trapezoidal law [20], perfectly plastic law [21], polynomial law [22], exponential model [23], and bilinear law [15, 19, 24-26]. ABAQUS only supports exponential and bilinear models. In our research, for simplicity the bilinear model has been chosen. This choice will make it easier and faster to integrate the software model to SLA machine and is in line with our goal of designing an online monitoring system that can assess the stress at the cured object as fast as possible. The area under the traction-separation curve is also equal to the fracture toughness G_c . CZM is simple and can simulate both crack on set and propagation in one model. On the other hand, CZM formulas can easily be implemented in finite element analysis software packages.

2.1. Calculation of Stiffness Parameters

Different methods have been proposed for calculation of the stiffness parameters. Daudeville et al. presented the relationship between stiffness parameters and the thickness and elastic modulus [27]. Zou et al. also introduce the range of 10^4 and 10^7 times the value of the interfacial strength per unit length to be the approximate amount of stiffness coefficients [28]. The effect of mesh size of the cohesive finite element on the delamination of the plies was investigated by Turon et al. [10]. Tvergaard proposed the first de-cohesion model based on both normal and tangential separation [20]. Afterwards, a traction-separation response model is widely used to study the cohesive and damage property. In our work, the initial response of the cohesive behavior is linear until a damage initiation is met. K_i for a bi-linear traction-separation law is defined in Eq. 2.

$$K_i = \frac{t_i}{\delta_i^0} \quad (2)$$

Where δ_i^0 is the critical separation for damage initiation. The value of the penalty stiffness should be high enough to prevent interpenetration of the crack faces. Equation 3 used by Turon et al. to calculate the amount of K .

$$K \geq \alpha \frac{E}{t} \quad (3)$$

Where α is a parameter larger than 1 (50 is recommended) and t is the thickness of the plies adjacent to the interaction surface. This method however is useful for composite materials where both sub-laminates (plies) adjacent to the cohesive surface are fabricated from the same material and have equal thickness. In our case, however, the two sub-laminates are from different materials and have different thicknesses. So we improved a method to calculate a t_n^0 and δ_n^0 . Having t_n^0 and δ_n^0 , the value of K is calculated using Eq. 2. In order to calculate the cohesive and damage parameters, a set of physical experiments have been performed to investigate the separation force of a cured layer based on a coated PDMS film. The setup for measuring the pulling force is shown in Fig. 5.

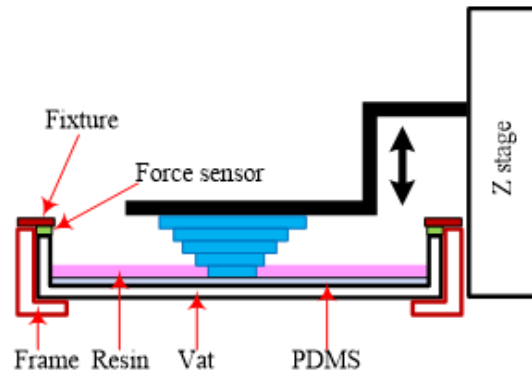


Figure 5. Experimental setup for studying the part separation forces

Two FlexiForce sensors (Tekscan, South Boston, MA) with a range of 0-25 lbs are sandwiched between the fixture and the vat. Since the vat is free at the bottom and the side, and only fixed at the top, the pulling force by the part will be transferred to the sensors when the platform rises. The two sensors are connected to a microcontroller, which can record the sensors' readouts at over 3 KHz. In the experiments, we first use a given mask image to build a certain number of layers (e.g. 25 layers). We then begin to record the separation force in the building process of the next few layers. For each layer, after the designed mask image has been exposed for a certain time, the platform is raised up slowly at 0.6 mm/sec and the readouts of the two sensors are then recorded. Different image patterns with the same area are designed. Figure 6 shows the measured separation forces of a sensor for different patterns. The horizontal axis indicates the distance in the z-direction (in the unit of $10 \mu\text{m}$), and the vertical axis indicates the recorded pulling force (in ounce).

The area of the test pattern is 625 mm^2 . As can be seen from Fig. 6, for a shape with a cross section of square, the damage initiation starts at $\delta_n^0 = 0.4 \text{ mm}$ which is associated with the peak force of 80 oz. (22.24 N). Therefore, the amount of stress when damage is initiated is $t_n^0 = 22.24(\text{N}) / 625(\text{mm}^2) = 0.036 \text{ (MPa)}$, and the stiffness parameter is $K = 0.036(\text{N/mm}^2) / 0.4(\text{mm}) = 0.09 \text{ (MPa)}$.

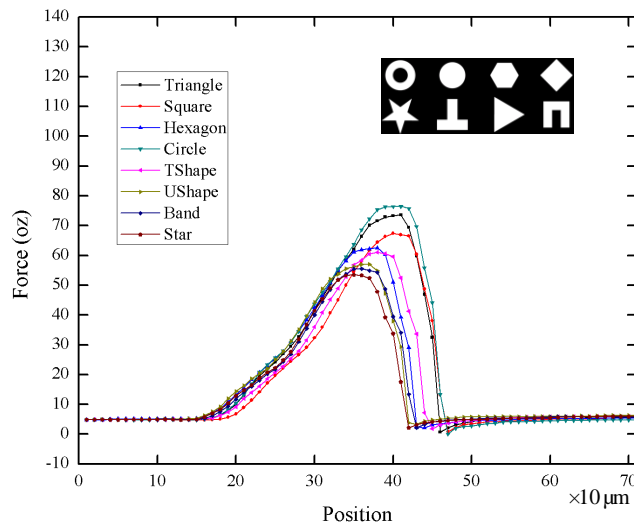


Figure 6. Pull force – Position plot for bottom-up SLA
(Courtesy of Zhou et al.)

2.2. Calculation of Damage Parameters

Damage modeling is used to simulate the degradation and eventual failure of the bond between the two cohesive surfaces. It consists of two parts: (1) damage initiation; (2) damage evolution. Damage initiation starts when the traction meets a criterion, and the damage evolution is controlled by either a linear or exponential behavior in ABAQUS.

2.2.1 Damage initiation criterion. A quadratic traction criterion has been chosen to define the damage initiation. In our model, damage is initiated when a quadratic traction function involving the contact stress

ratios reach the value of one.

$$\left\{ \frac{t_n}{t_n^0} \right\}^2 + \left\{ \frac{t_s}{t_s^0} \right\}^2 + \left\{ \frac{t_t}{t_t^0} \right\}^2 = 1 \quad (4)$$

According to the experiment that was described in section 2.1, the damage criterion is $t_n^0 = 0.036$ MPa.

2.2.2 Damage evolution. Benzeggah *et al.* have evaluated the initiation of cracking and delamination growth in a unidirectional glass/epoxy composite under mode I, mode II, and mixed mode I+II static loading [29]. Camanho *et al.* have also developed the rules and regulations of delamination of cohesive plies [30]. They proposed a single relative displacement-based damage parameter for softening law that controls the damage evolution. Damage evolution law is the rate at which the cohesive stiffness is degraded after the damage initiation has occurred. D is the scalar damage variable which has a value between 0 and 1. During damage evolution, D monotonically evolves from 0 to 1 upon further loading after initiation of damage [31]. The relationship between the stress components and scalar damage variable is:

$$t_n = \begin{cases} (1 - D)\bar{t}_n, & \bar{t}_n \geq 0 \\ \bar{t}_n & \text{Otherwise} \end{cases} \quad (5)$$

$$t_s = (1 - D)\bar{t}_s \quad (6)$$

$$t_t = (1 - D)\bar{t}_t \quad (7)$$

Where \bar{t}_n , \bar{t}_s , and \bar{t}_t are the contact stress components predicted by the elastic traction separation behavior for the current separation without damage [31].

As mentioned before, the softening behavior in our model has been chosen to be linear and ABAQUS ensures that the area under the linear or the exponential damage response is equal to the fracture energy. Linear energy evolution can be expressed as:

$$D = \frac{\delta_m^f (\delta_m^{\max} - \delta_m^0)}{\delta_m^{\max} (\delta_m^f - \delta_m^0)} \quad (8)$$

Where $\delta_m^f = 2G^c / T_{\text{eff}}^0$ and δ_m^{\max} is the maximum value of the effective separation and T_{eff}^0 is the effective traction at damage initiation. As mentioned before, the amount of fracture energy for damage evolution will be the area under the triangle. In our case, $\delta_n^f = 0.48$ mm, thus $G^c = (1/2)(0.48)(0.036) = 8.64 \times 10^{-3}$ (N/mm). The viscosity coefficient for damage stabilization has been considered 10^{-15} . In section 3, a method will be proposed to optimize these cohesive and damage parameters using MATLAB.

3. PARAMETERS OPTIMIZATION

This section covers the procedure of development of an optimization model to estimate stiffness parameters of the cohesive layer between photopolymer solid and the PDMS silicone film as these parameters cannot be calculated using direct mechanical tests and should be extracted from experimental data. The general idea is minimizing the error between experimental data and ABAQUS predication as the parameters values are changed dynamically in ABAQUS. An objective method should be developed to evaluate and compare the performance of the various models. We have used mean squared error as objective method to calculate the error between experimental and predicted data. Similar models have been developed employing finite difference method [32], as well as finite element method [33]. Lei *et al.* have also developed their own code using MATALB and ABAQUS to evaluate material parameters of biological soft tissues [34].

We have used MATLAB to program a code that satisfies all we discussed previously as the optimization procedure. MATALB provides an excellent environment for such a task as it can call any external command or executable file [34]. The developed MATALB code executes ABAQUS to obtain predicted finite element results and reads the results from the ABAQUS output file. It also executes a text file to read the experimental data and modifies the ABAQUS input file through a special code to change the amount of parameters values dynamically. It generates a special input file containing parameter values for each run and that input file is

connected to the main input file using the PYTHON command *INCLUDE. The optimization procedure uses mean squared error as objective function to calculate the error and the minimum value will be calculated using *fmincon* function. The displacement in normal direction is considered as our desirable variable to study the cohesive behavior and optimize parameters. The optimization procedure can be summarized into four steps:

1. Reading experimental data: The displacement values for nodes of the target (real) case are considered experimental data. These values have been stored in a text file. MATLAB reads those values by loading that text file.
2. Calculating predicted data: Running ABAQUS for different values of a parameter and reading the predicted results from ABAQUS output (.dat) file. We have considered different meshing policies of the same model as different cases. Then by choosing one of them as a target or experimental case, the amount of displacement for every node in non-target cases will be estimated from the displacement of the nodes near that location in target case using interpolation.
3. Calculation of error: The difference between the displacement values is calculated using a mean squared error objective function:

$$100 \frac{\sqrt{\sum_{i=1}^n (e_i - p_i)^2}}{\sqrt{\sum_{i=1}^n e_i^2}} \quad (9)$$

Where e_i refers to experimental data and p_i refers to a predicted data.

4. Plotting the error over different values of the parameter we want to optimize and calculating the optimum value using optimization formulas.

A limitation of this procedure is that it may yield a local minimum if the “parameter under study – error” plot is not convex. Global optimization or heuristic methods can be employed to overcome this problem. However, these methods are expensive in terms of computation and are not useful in our case as we want to shorten the fabrication time and complete the force analysis in the least possible time. We have used different functions e.g. Cubic3, ScatteredInterpolant, and 10th degree polynomial to perform interpolation on scattered error data. In addition, running the code for a large range of parameters at first to get an overall idea of the location of the global minimum and selection of the best initial point will also help. This method can integrate MATLAB and ABAQUS and if needed also other software which makes it an accessible and powerful tool to use for evaluation of mechanical parameters based on experimental data. We started developing the optimization code from a very simple model. Optimization of mechanical parameters for a static bottom-up model without considering the cohesive behavior was chosen as the first step.

3.1. Static Bottom-up Model without Considering the Cohesive Behavior

In this step, the actual bottom-up model is used to optimize parameters. All the mechanical properties and boundary conditions are same as the original model, except for the cohesive behavior. The cohesive interaction was removed and two parts were merged together instead. This is also a static simulation, so a static step was defined to eliminate the effect of the time. In original model, the photopolymer cube moves up at the constant velocity of 0.1 mm per second. In this step, however, this fixed velocity boundary condition should be replaced with a uniform pressure applied on top surface of the solid. The amount of pressure should be calculated in such a way that:

- The maximum stress at photopolymer solid should be less than the yield stress of photopolymer.
- The maximum displacement at the interface between two parts should be less than 1 mm which has been chosen based on experience.
- The maximum stress at the silicone film should be less than its fracture (tensile) strength.

The minimum amount of pressure for three criteria mentioned above is going to be chosen as the amount of pressure. The mechanical properties of photopolymer and PDMS silicone film are presented in Table 1.

Table 1. Mechanical properties of materials

Material	Young's modulus (MPa)	Poisson's ratio	Yield Stress (MPa)	Tensile Strength (MPa)
Photopolymer	2000	0.45	12	-
Silicone Film	0.36	0.5	-	2.24

The amounts of pressure equal to -8 MPa, -0.7 MPa, and -1.8 MPa satisfy the requirement 1, 2, and 3, respectively. Table 2 summaries the results of using these pressure values and whether they satisfy all the requirements or not. Green cells refer to satisfied requirements and yellow cells refer to unsatisfied requirements.

Table 2. Calculation of pressure

Criteria	P = -8 MPa	P = -0.7 MPa	P = -1.8 MPa
Max. Stress in Solid (<12 MPa)	11.76 MPa	1.04 MPa	2.23 MPa
Max. Displacement (<1 mm)	11.51 mm	0.97 mm	2.6 mm
Max. Stress in Film (<2.24 MPa)	9.93 MPa	0.87 MPa	2.69 MPa

Based on the results of Table 2, $P = -0.7$ MPa is a suitable amount for the pressure and it will not cause damage to the solid and film and also will move up the solid more than the amount required for complete delamination. Pressure equal to -0.7 MPa, however, was not suitable for the case we remeshed the model. So the same procedure was repeated for adaptively remeshed model and $P = -0.5$ MPa was chosen. The amount of pressure equal to 0.5 MPa produces the maximum stress of 2.667 MPa in the solid which is less than solid's yield stress (12 MPa). The maximum amount of stress in the film will be 1.7 MPa for this amount of pressure which is less than the film's tensile strength (2.24 MPa). The maximum displacement at the interface between two parts corresponding to $P = -0.5$ MPa will be 0.94 mm.

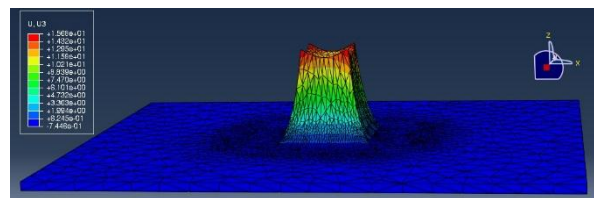


Figure 7. Displacement (U3) contour for $P = -0.5$ MPa

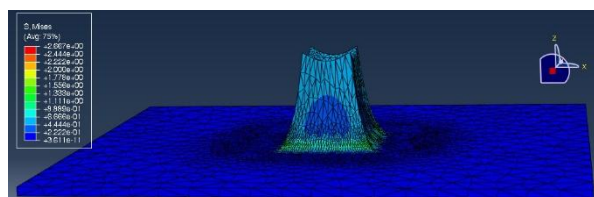


Figure 8. Stress contour for $P = -0.5$ MPa

The optimization was done for four different scenarios:

Scenario 1: Changing Young's modulus of photopolymer while other parameters are fixed.

Scenario 2: Changing Young's modulus of silicone film while other parameters are fixed.

Scenario 3: Changing Poisson's ratio of photopolymer while other parameters are fixed.

Scenario 4: Changing Poisson's ratio of silicone film while other parameters are fixed.

To generate different cases from the original model, different remeshing policies were used to get different number of elements. The film was partitioned into two different portions in order to assign smaller error distribution percentage to the portion of film near the interface. Different cases were created by assigning different error distribution percentages (4%, 4.5%, 5%, 5.5%, 6%, 8%, and 10%) to the solid and inner portion of the film. The uniform error distribution percent for the outer part of the film is 10% for all cases. The case with error distribution percentages of 5% for solid and inner film and 10% for outer film was chosen as our target experimental case. The optimization plots for 6% error model for different scenarios are shown in Fig. 9

(a~d) as an example.

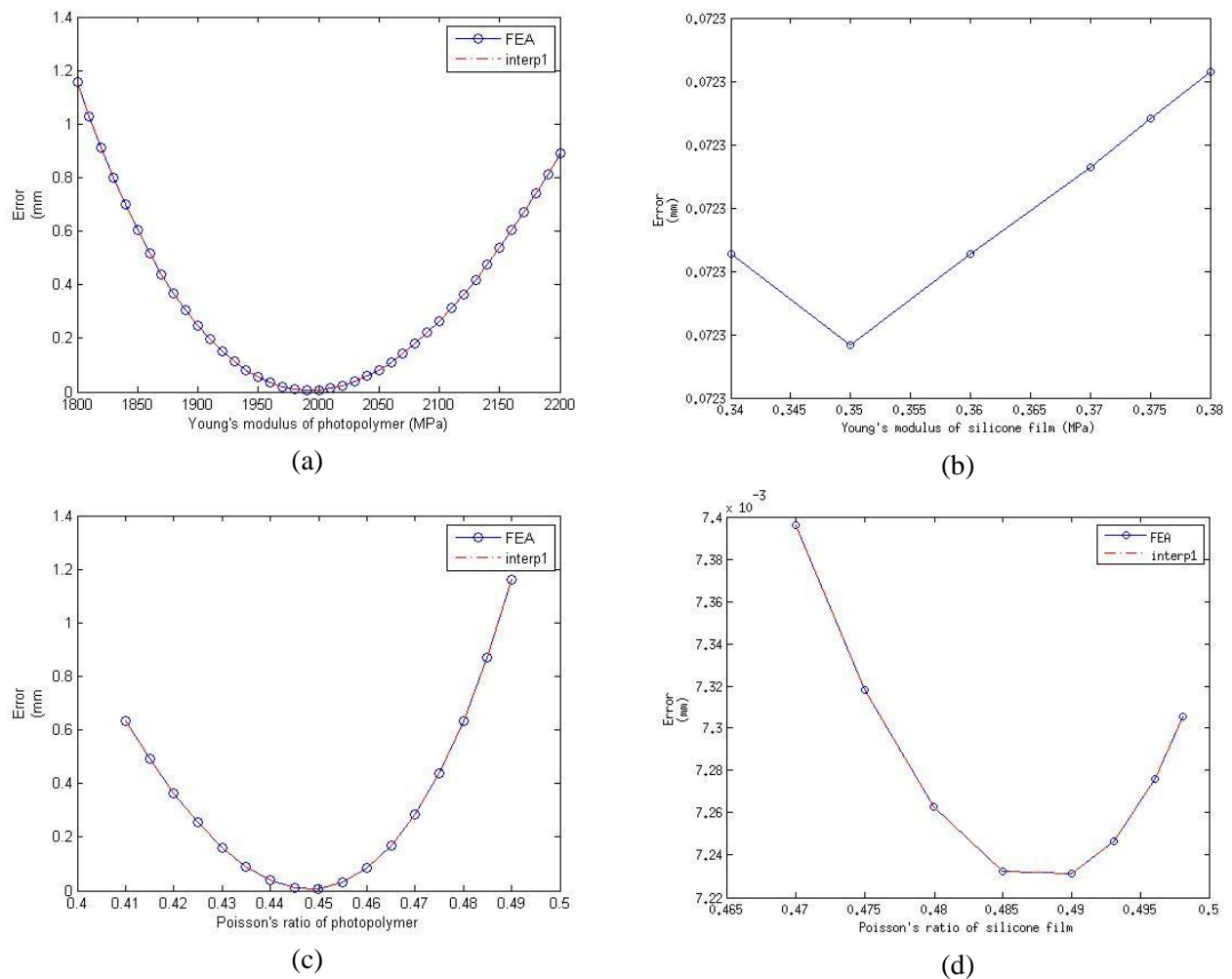


Figure 9. Results of the optimization for 6% error distribution model: (a) Young's modulus of photopolymer ($1800 < E < 2200$); (b) Young's modulus of silicone film ($0.34 < E < 0.38$); (c) Poisson's ratio of photopolymer ($0.4 < \nu < 0.5$); (d) Poisson's ratio of silicone film ($0.465 < \nu < 0.5$)

Table 3 contains the optimization results for four different elastic parameters evaluated in four different scenarios.

Table 3. Optimization results for static bottom-up model without cohesive behavior

Model Number	Percentage	Scenario 1	Scenario 2	Scenario3	Scenario4
1	4% - 10%	2000	-	0.45	0.4888
2	4.5% - 10%	2000	-	0.45	0.485
3	5% - 10%	2000	0.36	0.45	0.49
4	5.5% - 10%	2000	-	0.45	0.4886
5	6% - 10%	1991.4	-	0.45	0.486
6	8% - 10%	1989.9	-	0.445	0.4871
7	10% - 10%	1970	-	0.44	0.4871

3.2. Pseudo-dynamic Bottom-up Model Considering the Cohesive Behavior

At this step, the optimization was done for the cohesive stiffness parameters (K_i) of the original model. The model was run for 20 seconds. However, considering the time in the model will increase the time of adaptivity remeshing dramatically. First, the model was run with the remeshing policies of 8%, 15%, and 18% for solid, inner portion of the film, and outer portion of the film, respectively. The remeshing was repeated 100

times. Figure 10 shows the target uniform error distribution values, as well as the amount of error that each part will reach during different iterations. As can be seen in Fig. 10, not all the criteria have been satisfied. Increasing the number of iterations may satisfy all of them, but it will take hours to be fulfilled. On the other hand, the remeshing results are satisfactory and the mesh around the cohesive interface is so tense. The deformed displacement contour of 3D model is also shown in Fig. 11. The displacement contour is symmetric both on the surface and inside the film. As a result, we chose to continue the optimization process with a 2D model of bottom-up cohesive AM.

Using 2D model will reduce the number of nodes and eventually the optimization time. A 2D model was developed based on the geometry and properties of the original model. The process of remeshing was done for three iterations. Figure 12 shows the amount of error percentage for each iteration. Starting with 10% and 15% as our uniform error distribution targets, 8%, 15%, and 18% have been reached after three iterations for solid, inner portion of film, and outer portion of film, respectively. As can be seen in Fig. 12, the only criterion that was satisfied is the 8% for the solid. However, the final error percentages for the film portions are so close to the target. Due to the limited capacity of the computer system we used, we could not repeat the remeshing process more than three times. Figure 12 shows the change in the model mesh after each iteration. The third iteration has the behavior most similar to the real case, hence, it was chosen as the target experimental test. The first and second iterations are going to be compared to this case.

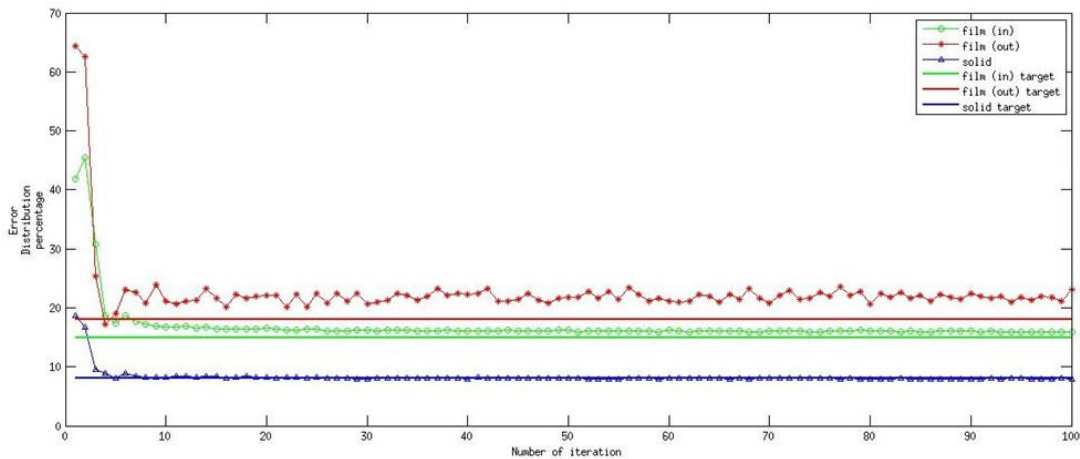


Figure 10. Uniform error percentage – Number of iterations plot for 3D model

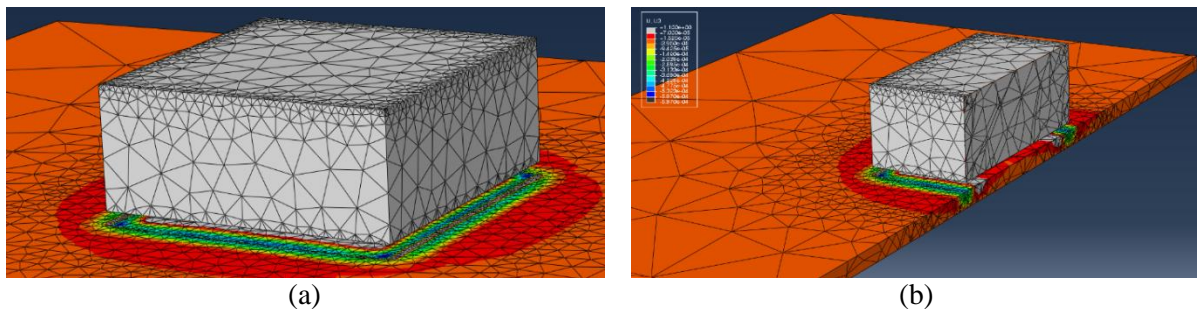


Figure 11. Deformed displacement contour of 3D cohesive model; (a) overall view; (b) cut view.

ABAQUS/Standard finds the converged solution of the model in different time increments for each step. The values of variables such as stress, strain, displacement etc. can be reported for every node and/or element at the end of each increment in ABAQUS output (.dat) file. Formerly we optimized the model in static phase, so we only could report the amounts of variables once at the end of the simulation. Now we have different increments and we need to identify one or more points during moving up step to extract the results at those points. The crack initiation time is the most important milestone as the nodes nearly experience the maximum amount of stress at this point. To find the crack initiation time,

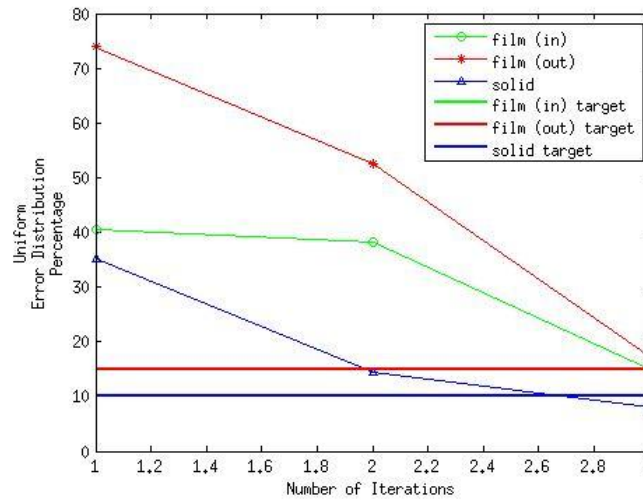


Figure 12. Uniform error percentage – number of iterations plot for 2D model

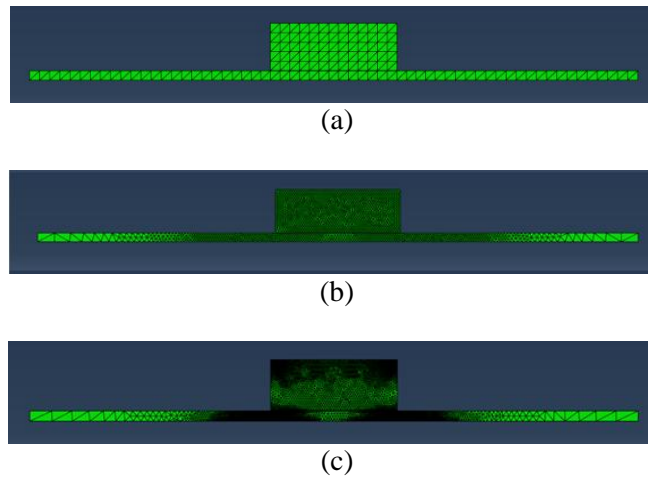


Figure 13. Undeformed displacement contours for 2D model;
(a) 1st iteration; (b) 2nd iteration; (c) 3rd iteration

stress was plotted for different nodes on interface of the solid and PDMS silicone film over the time. Figure 14 shows the stress – time plot for one of the nodes. The maximum stress happens at a time around 4 seconds and the complete delamination at around 5.5 seconds. Other nodes on the interface have the exact same behavior. In order to report the displacement amounts at exact crack initiation and complete delamination times, we divided the 20 seconds moving up step into three parts: (1) crack initiation step (4 seconds); (2) crack evolution step (1.5 seconds); (3) moving up step (14 seconds). Using *NODE PRINT command in input file, the amounts of displacement in normal direction for desired increments of every step. However, displacement was only reported for a special node set on the cohesive interaction between the two objects not all the nodes to decrease the computational time. This target area experiences the most amount of stress as well as the largest displacement.

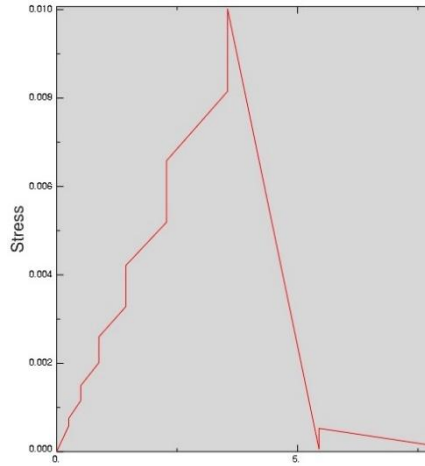


Figure 14. Stress – time plot for a single node on the cohesive area of the film

The results of optimization for the first and second iterations are shown in Fig. 15. The optimized value of K is equal to 0.0855 N/mm^3 for the 1st iteration and 0.09455 N/mm^3 for the 2nd iteration.

3.3. Validation of the Optimization Model

The main target of developing an optimization model is to evaluate the cohesive stiffness parameters. However, the optimized values should help to improve the performance of the models with coarser meshes which is helpful in reduction of the total time of analysis once the ABAQUS model is integrated into the SLA machine. To investigate the validation of optimization model, the 2nd iteration was run with the optimized value of cohesive stiffness ($k = 0.09455 \text{ N/mm}^3$). The results of the simulation in terms of displacement were plotted over the cohesive interface for different increments of time. The same procedure was done for the results of 3rd iteration with non-optimized stiffness parameter ($k = 0.09 \text{ N/mm}^3$). It is expected that the model with coarser mesh (2nd iteration) should produce the similar results to the model with finer mesh (3rd iteration), once provided with the optimized parameters. Figure 16 shows the results of displacement over the time for both cases.

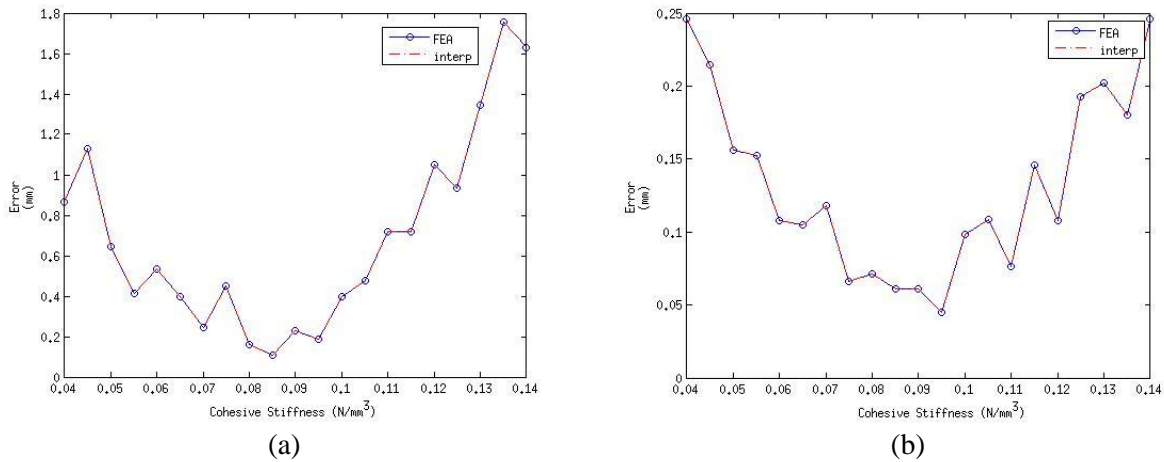
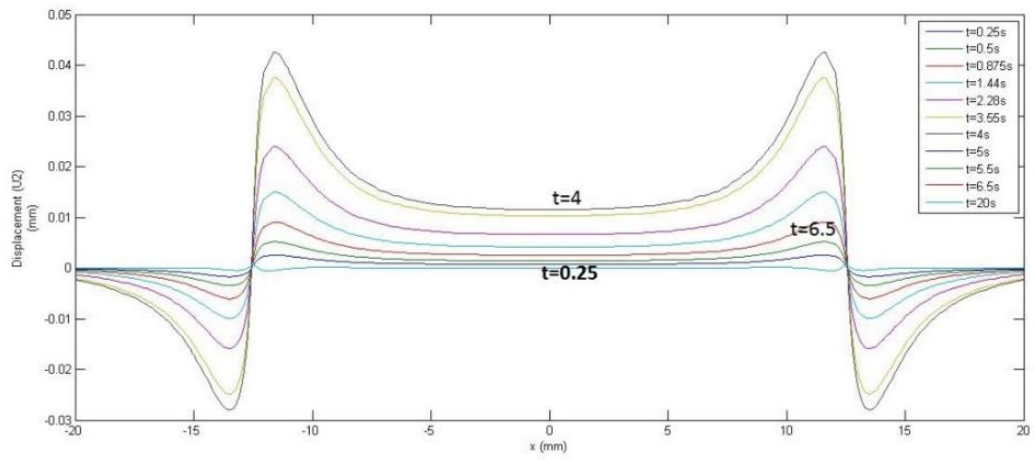
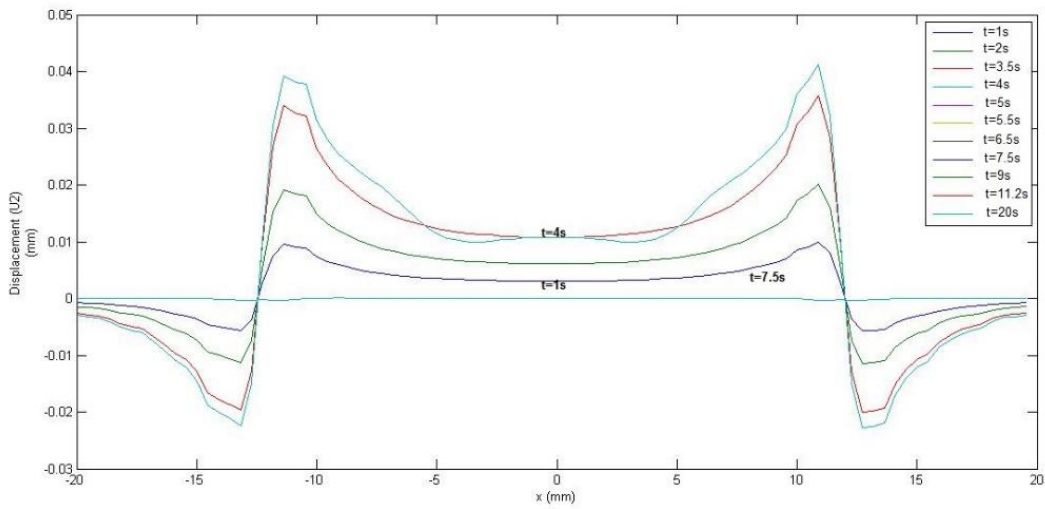


Figure 15. Results of the optimization for remeshing iterations 1 and 2;
 (a) 1st iteration ($0.04 < K < 0.14$); (b) 2nd iteration ($0.04 < K < 0.14$)



(a)



(b)

Figure 16. Displacement – x plot for cohesive interface over the time;
 (a) 3rd iteration with non-optimized K ; (b) 2nd iteration with optimized K .

As can be seen from Fig. 16, the behavior of the two cases is the same both quantitatively and qualitatively. They both reach a maximum displacement of nearly 0.04 mm and their displacement behavior follows a certain pattern. First, it gradually increase until it gets to the maximum displacement at $t = 4$ seconds; then a sudden drop (or softening with sharp slope) happens which is the result of the quick degradation of cohesive effect of surface elements in crack evolution stage. Fig. 16 (a~b) testifies that the proposed optimization method is valid and can be used to increase the time efficiency of the final online force control system.

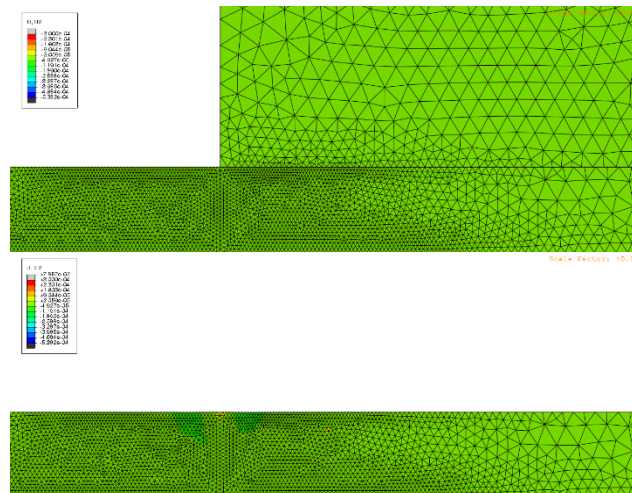
4. MODEL RESULTS

The goal of this paper is developing a FEM model using ABAQUS to model the behavior of the cohesive delamination at the interface of a photopolymer solid and a PDMS silicone film in a bottom-up projection-based additive manufacturing process. This research is motivated by the fact that the pulling up force plays an important role in the final quality of the parts and the reliability of the bottom-up projection-based process. However, the research work is not well conducted yet in this area. To fill this gap, our goal is developing a mechanics-based closed-loop force monitoring system. To do that, the first step was to study and model the cohesive delamination and peeling. We simulated the bottom-up projection-based process in ABAQUS/Standard and evaluated the cohesive stiffness parameters using an optimization method which integrates ABAQUS and MATALB and optimizes the mechanical parameters using a mean squared error function. Running the model with the evaluated parameters, the cohesive behavior result is shown in Fig. 17.



Figure 17. Magnified cohesive behavior

To give a better view of the displacement, the movement in y direction is magnified 100 times. The results show that the behavior of the cohesive model is in line with what it is expected from theory and the experience. Elements with cohesive property follow the bi-linear traction-separation law perfectly. The sudden degradation of the cohesive effect which also can be expected from experience has been achieved very well. The results presented in section 3.3 also testify the validity of the optimization model. Figure 18 also shows the delamination process over the time.



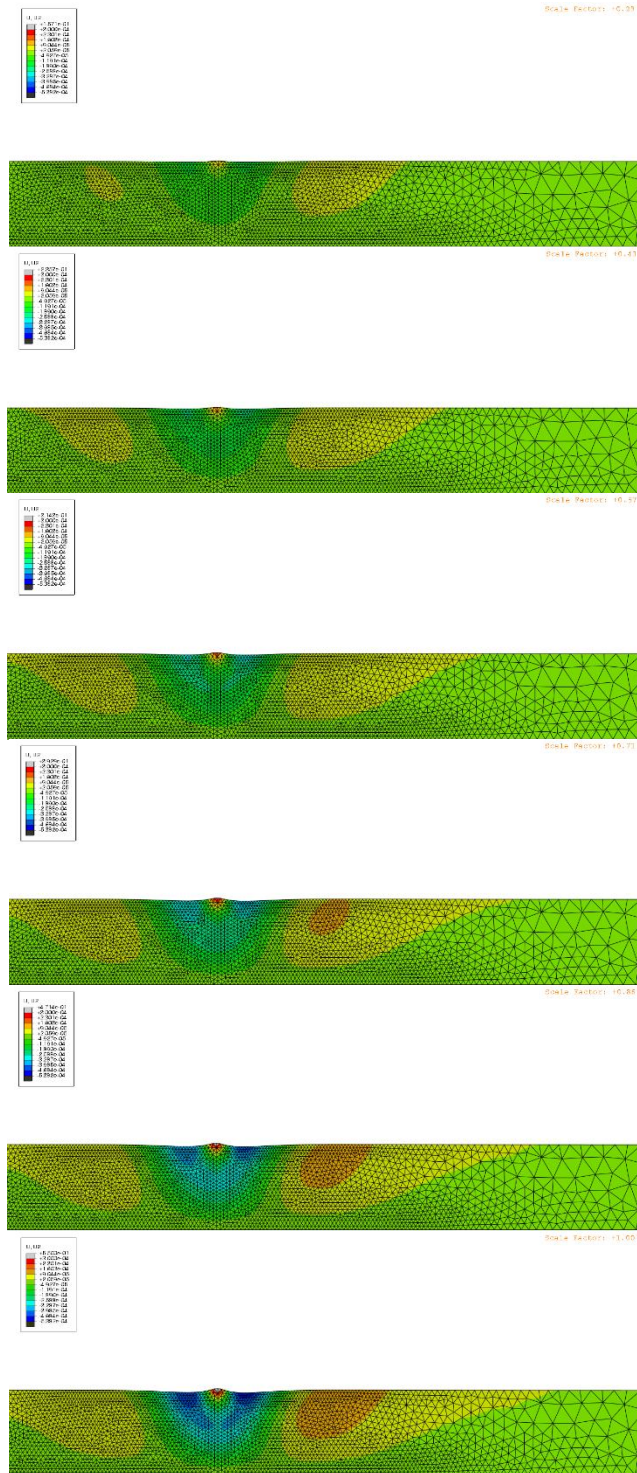


Figure 18. Delamination over the time

5. CONCLUSION AND FUTURE WORK

The result of this work would be very influential in manufacturing area, since this method will improve the fabrication speed and part quality. However, simplification of the final FEM model in such a way that the simulation results be satisfactory and integrating this model into the bottom-up projection-based stereolithography machine will be very challenging. Therefore, this research is very helpful and at the same time lots of research work is expected to be done in the future. This research has made the following contributions:

- (1) Utilize finite element method to model the cohesive delamination process in bottom-up projection-based additive manufacturing process which will be used as a basis to develop an online closed-loop force monitoring system.
- (2) Establish an optimization model to evaluate the mechanical parameters that cannot be calculated directly from closed formulas or mechanical tests and need to be estimated from experimental results.

Designing an online force monitoring system for bottom-up projection-based model is very challenging and will be an ongoing research topic. Even this very first task obtained some results; it has lots of limitations and still at preliminary stage. More comparisons similar to the optimized iteration 2 and iteration 3 should be done to confirm the optimization method. It also has been assumed that the silicone film sticks to the resin tank and its bottom surface is fixed. This assumption needs to be validated. The feasibility of defining film as a hyper-elastic material instead of an elastic material in terms of simulation cost should also be investigated. In order to get a more realistic model, the cohesive model should be completed applying stochastic parameters.

REFERENCES

- [1] Economist, 2011, "Print me a Stradivarius: How a new manufacturing technology will change the world," <http://www.economist.com/node/18114327>.
- [2] Bourell, D. L., Leu, M. C., and Rosen, D. W., 2009, "Roadmap for additive manufacturing: identifying the future of freeform processing," The University of Texas, Austin.
- [3] Zhou, C., Chen, Y., Yang, Z. G., and Khoshnevis, B., 2011, "Development of a multi-material mask-image-projection-based stereolithography for the fabrication of digital materials."
- [4] Melchels, F. P. W., Feijen, J., and Grijpma, D. W., 2010, "A review on stereolithography and its applications in biomedical engineering," *Biomaterials*, 31(24), pp. 6121-6130.
- [5] Huang, Y.-M., and Jiang, C.-P., 2005, "On-line force monitoring of platform ascending rapid prototyping system," *Journal of materials processing technology*, 159(2), pp. 257-264.
- [6] Denken, 1997, "SLP-4000 Solid Laser Diode Plotter, Product Brochure."
- [7] Monneret, S., Loubere, V., and Corbel, S., 1999, "Microstereolithography using a dynamic mask generator and a noncoherent visible light source," *International Society for Optics and Photonics*, pp. 553-561.
- [8] Pan, Y., Chen, Y., and Zhou, C., "Fast Recoating Methods for the Projection-based Stereolithography Process in Micro-and Macro-Scales."
- [9] Krueger, R., 2004, "Virtual crack closure technique: history, approach, and applications," *Applied Mechanics Reviews*, 57(2), pp. 109-143.
- [10] Turon, A., Davila, C. G., Camanho, P. P., and Costa, J., 2007, "An engineering solution for mesh size effects in the simulation of delamination using cohesive zone models," *Engineering Fracture Mechanics*, 74(10), pp. 1665-1682.
- [11] Schellekens, J. C. J., and De Borst, R., 1993, "A non-linear finite element approach for the analysis of mode-I free edge delamination in composites," *International Journal of Solids and Structures*, 30(9), pp. 1239-1253.
- [12] Allix, O., Ladeveze, P., and Corigliano, A., 1995, "Damage analysis of interlaminar fracture

- specimens," *Composite Structures*, 31(1), pp. 61-74.
- [13] Allix, O., and Corigliano, A., 1996, "Modeling and simulation of crack propagation in mixed-modes interlaminar fracture specimens," *International Journal of Fracture*, 77(2), pp. 111-140.
- [14] Chaboche, J. L., Girard, R., and Schaff, A., 1997, "Numerical analysis of composite systems by using interphase/interface models," *Computational Mechanics*, 20(1-2), pp. 3-11.
- [15] Mi, Y., Crisfield, M. A., Davies, G. A. O., and Hellweg, H. B., 1998, "Progressive delamination using interface elements," *Journal of composite materials*, 32(14), pp. 1246-1272.
- [16] Chen, 1999, "Predicting progressive delamination of composite material specimens via interface elements," *Mechanics of composite materials and structures*, 6(4), pp. 301-317.
- [17] Alfano, G., and M. A. Crisfield. "Finite element interface models for the delamination analysis of laminated composites: mechanical and computational issues." *International journal for numerical methods in engineering* 50.7 (2001): 1701-1736.
- [18] Goyal, V. K., Johnson, E. R., and Dávila, C. G., 2004, "Irreversible constitutive law for modeling the delamination process using interfacial surface discontinuities," *Composite Structures*, 65(3), pp. 289-305.
- [19] Turon, A., Camanho, P. P., Costa, J., and Dávila, C. G., 2006, "A damage model for the simulation of delamination in advanced composites under variable-mode loading," *Mechanics of Materials*, 38(11), pp. 1072-1089.
- [20] Tvergaard, V., and Hutchinson, J. W., 1992, "The relation between crack growth resistance and fracture process parameters in elastic-plastic solids," *Journal of the Mechanics and Physics of Solids*, 40(6), pp. 1377-1397.
- [21] Cui, W., and Wisnom, M. R., 1993, "A combined stress-based and fracture-mechanics-based model for predicting delamination in composites," *Composites*, 24(6), pp. 467-474.
- [22] Needleman, A., 1987, "A continuum model for void nucleation by inclusion debonding," *Journal of applied mechanics*, 54(3), pp. 525-531.
- [23] Xu, X. P., and Needleman, A., 1994, "Numerical simulations of fast crack growth in brittle solids," *Journal of the Mechanics and Physics of Solids*, 42(9), pp. 1397-1434.
- [24] Reedy, E. D., Mello, F. J., and Guess, T. R., 1997, "Modeling the initiation and growth of delaminations in composite structures," *Journal of Composite Materials*, 31(8), pp. 812-831.
- [25] Camanho, P. P., Davila, C. G., and De Moura, M. F., 2003, "Numerical simulation of mixed-mode progressive delamination in composite materials," *Journal of composite materials*, 37(16), pp. 1415-1438.
- [26] Turon, A., Camanho, P. P., Costa, J., and Dávila, C. G., 2004, "An interface damage model for the simulation of delamination under variable-mode ratio in composite materials," *NASA/Technical Memorandum*, 213277.
- [27] Daudeville, L., Allix, O., and Ladeveze, P., 1995, "Delamination analysis by damage mechanics: some applications," *Composites Engineering*, 5(1), pp. 17-24.
- [28] Zou, Z., Reid, S. R., Li, S., and Soden, P. D., 2002, "Modelling interlaminar and intralaminar damage in filament-wound pipes under quasi-static indentation," *Journal of composite materials*, 36(4), pp. 477-499.
- [29] Benzeggagh, M. L., and Kenane, M., 1996, "Measurement of mixed-mode delamination fracture toughness of unidirectional glass/epoxy composites with mixed-mode bending apparatus," *Composites Science and Technology*, 56(4), pp. 439-449.
- [30] Camanho, P. P., and Dávila, C. G., 2002, "Mixed-mode decohesion finite elements for the simulation of delamination in composite materials," *NASA-Technical paper*, 211737(1), p. 33.
- [31] Song, K., Dávila, C. G., and Rose, C. A., 2008, "Guidelines and parameter selection for the simulation of progressive delamination," pp. 1-15.

- [32] Ateshian, G. A., Warden, W. H., Kim, J. J., Grelsamer, R. P., and Mow, V. C., 1997, "Finite deformation biphasic material properties of bovine articular cartilage from confined compression experiments," *Journal of biomechanics*, 30(11), pp. 1157-1164.
- [33] Laible, J. P., Pflaster, D., Simon, B. R., Krag, M. H., Pope, M., and Haugh, L. D., 1994, "A dynamic material parameter estimation procedure for soft tissue using a poroelastic finite element model," *Journal of biomechanical engineering*, 116(1), pp. 19-29.
- [34] Lei, F., and Szeri, A. Z., 2007, "Inverse analysis of constitutive models: biological soft tissues," *Journal of biomechanics*, 40(4), pp. 936-940.